Published in final edited form as:
Phys Med Biol. 2014 October 7; 59(19): L1–L13. doi:10.1088/0031-9155/59/19/L1.

3D Ultrafast Ultrasound Imaging In Vivo

Jean Provost, **Clement Papadacci**, **Juan Esteban Arango**, **Marion Imbault**, **Jean-Luc Gennisson**, **Mickael Tanter***, and **Mathieu Pernot***
ESPCI ParisTech, PSL Research University, Institut Langevin, 1 rue Jussieu, F-75005, Paris, France; CNRS, Institut Langevin, 1 rue Jussieu, F-75005, Paris, France; INSERM, Institut Langevin, 1 rue Jussieu, F-75005, Paris, France; Université Paris Diderot, Sorbonne Paris Cité, Institut Langevin, UMR 7587, 1 rue Jussieu, F-75005, Paris, France; Sorbonne Universités, UPMC Univ Paris 06, UMR 7587, Institut Langevin, 1 rue Jussieu, F-75005, Paris, France

Abstract

Very high frame rate ultrasound imaging has recently allowed for the extension of the applications of echography to new fields of study such as the functional imaging of the brain, cardiac electrophysiology, and the quantitative real-time imaging of the intrinsic mechanical properties of tumors, to name a few, non-invasively and in real time. In this study, we present the first implementation of Ultrafast Ultrasound Imaging in three dimensions based on the use of either diverging or plane waves emanating from a sparse virtual array located behind the probe. It achieves high contrast and resolution while maintaining imaging rates of thousands of volumes per second. A customized portable ultrasound system was developed to sample 1024 independent channels and to drive a 32×32 matrix-array probe. Its capability to track in 3D transient phenomena occurring in the millisecond range within a single ultrafast acquisition was demonstrated for 3-D Shear-Wave Imaging, 3-D Ultrafast Doppler Imaging and finally 3D Ultrafast combined Tissue and Flow Doppler. The propagation of shear waves was tracked in a phantom and used to characterize its stiffness. 3-D Ultrafast Doppler was used to obtain 3-D maps of Pulsed Doppler, Color Doppler, and Power Doppler quantities in a single acquisition and revealed, for the first time, the complex 3-D flow patterns occurring in the ventricles of the human heart during an entire cardiac cycle, and the 3-D *in vivo* interaction of blood flow and wall motion during the pulse wave in the carotid at the bifurcation. This study demonstrates the potential of 3-D Ultrafast Ultrasound Imaging for the 3-D real-time mapping of stiffness, tissue motion, and flow in humans in vivo and promises new clinical applications of ultrasound with reduced intra- and inter-observer variability.

Keywords

Ultrafast Ultrasound Imaging; 3-D Ultrasound Imaging; Volumetric Imaging; Blood Flow; Tissue Velocity; Tissue Doppler; Pulsed Doppler; Color Doppler; Power Doppler; Cardiac Imaging; Real-time Volumetric Imaging

Address correspondence to: Mathieu Pernot, Institut Langevin, 1 rue Jussieu, 75005, Paris, France. Tel: +33(0)180963040, Fax: +33(0)180963355, Mathieu.pernot@espci.fr.
*MP and MT are co-last authors

Europe PMC Funders Author Manuscripts

Over the last few years, 2-D ultrasound imaging has undergone important technical improvements with the advent of software-based systems that enable the implementation of ultra-high frame rate imaging techniques: up to 20 000 frames/s are achieved, as opposed to the 50-200 frames/s used in traditional clinical systems. When such high frame rates are achieved in a large field of view, e.g., by using either plane wave ultrasound transmissions (Sandrin et al., 1999; Tanter et al., 2002), diverging wave transmissions (Couade et al., 2009; Honjo et al., 2010; Clement Papadacci et al., 2014; Provost et al., 2011b) or gating techniques (Pernot et al., 2007a; Provost et al., 2010; Wang et al., 2008), they allow for the study of rapid phenomena, such as the propagation of artificially-induced shear waves (Bercoff et al., 2004; Sandrin et al., 2003) and natural waves in tissues, e.g., the electromechanical wave in the heart (Provost et al., 2011a) and the pulse wave in the blood vessels (Couade et al., 2010; Fujikura et al., 2007; Konofagou et al., 2011; Pernot et al., 2007b). For this reason, it corresponds to one of the three categories of wave interactions in the field of multi-wave imaging (Fink and Tanter, 2010). Moreover, such high frame rates improve temporal resolution, which in turn provides high-quality tissue motion and flow mapping. For example, estimating the heart tissue motion above 500 frames/s results in a five-fold improvement of the elastographic signal-to-noise ratio (Provost et al., 2012), while the increase in sensitivity of Ultrafast Doppler Imaging provides imaging of blood vessels with unprecedented resolution (Demené et al., 2014; Mace et al., 2011). These new techniques have bred entirely new fields of clinical applications for ultrasound imaging (Tanter and Fink, 2014), such as the quantitative characterization of tumors (Tanter et al., 2008), functional imaging of the brain (Macé et al., 2011; Osmanski et al., 2014), non-invasive imaging of cardiac electrophysiology (Provost et al., 2013), the study of the arterial stiffness in hypertension (Vappou et al., 2010), and high resolution vector flow imaging (Dort et al., 2012; Ekroll et al., 2013; Udesen et al., 2008; Yiu et al., in press) to name a few.

Applying these techniques in three dimensions would significantly broaden their scope of application. For example, both shear and natural wave propagation occur in three dimensions and their quantitative assessment can only be done in two dimensions at the cost of simplifying assumptions. This aspect is crucially important when attempting to identify a pacing site in the heart for the treatment of arrhythmias (Provost et al., 2013) or to detect the presence of mechanical anisotropy (Lee et al., 2012). Moreover, generalizing Ultrafast Doppler Imaging to three dimensions would allow for new fields of study to emerge such as, e.g., the quantitative, fully non-invasive angiography of complex networks of blood vessels and the imaging of the cardiac fiber orientation (C. Papadacci et al., 2014). Unfortunately, existing commercial 3-D ultrasound systems are typically relying on hardware-based focused ultrasound beams and thus limited to a few tens of volumes per second. Although many approaches have been proposed in the literature to perform high volume rate volumetric ultrasound imaging (Denarie et al., 2013; Perrin et al., 2012; Skaug et al., 2013), none, to our knowledge, provides sufficiently high volume rates to perform motion and blood flow measurement in an entire volume.

The concept of 3-D ultrafast imaging at thousands of volumes per second relies on the transmission of a small number of ultrasound defocussed waves that insonify the entire volume of interest. Dynamic focusing in receive is performed whereas the coherent synthetic summation of the ultrasonic volume acquired for each transmission allows the restoring of a

dynamic focus in transmit without compromising the ultrafast volume rate. Montaldo et al. applied this concept in 2D with plane wave transmissions, which resulted in coherent plane wave compounding (Montaldo et al. 2009) and can be used for the simultaneous mapping of both flow and tissue velocities (Ekroll et al., 2013) Recently, in the framework of ultrafast imaging of the human heart, we demonstrated the feasibility of compounding diverging waves using a sparse virtual array located behind the probe to achieve high frame rates and large signal-to-noise ratios in two dimensions in vivo at a limited cost in terms of resolution and contrast when compared to standard, low-frame-rate, focused imaging (Clement Papadacci et al., 2014). Building on previous theoretical studies of sparse virtual arrays (Hazard and Lockwood, 1999; Lockwood et al., 1998; Nikolov, 2001; Nikolov et al., 2010), we report herein on the development of 3-D Ultrafast Ultrasound Imaging based on the emission of diverging or plane waves emanating from virtual sources located behind a 2D-array ultrasound probe. By coherently compounding multiple emissions and by sampling the data of 1024 piezoelectric elements, we demonstrate that it is possible to perform 3-D ultrasound imaging at thousands of volumes per second with large contrast and high resolution, in humans in vivo.

In this work, we introduce 3-D Ultrafast Ultrasound Imaging and showcase potential clinical applications for cardiovascular imaging. More specifically, we describe the system architecture, validate the increase in contrast and resolution associated with coherently compounded emissions, and show the feasibility of motion estimation for shear-wave imaging in phantoms, of blood flow mapping in a full 3-D field of view of the human heart, and of the simultaneous 3-D mapping of both tissue and blood flow in the carotid artery near the bifurcation during the pulse wave propagation in vivo in humans.

Methods

System Infrastructure

A customized, programmable, 1024-channel ultrasound system was designed to drive a 32-by-35 matrix array centered at 3 MHz with a 50% bandwidth at −3 dB and a 0.3-mm pitch (Vermon, Tours, France). The 9^{th}, 17^{th} and 25^{th} lines were not connected resulting in a total number of active elements equal to 1024. The 1024 independent channels could be used simultaneously in transmission whereas receive channels were multiplexed to 1 of 2 transducer elements. Therefore, each emission was repeated twice, with the first half of the elements receiving during the first emission, and the second half of the elements receiving during the second emission.

All of the data processing such as delay-and-sum volume beamforming and flow and motion mapping were performed on graphic processing units (K6000, Nvidia, Santa Clara, CA) in a Matlab environment (2013b, Mathworks, Cambridge, MA). Real-time bi-plane beamforming was also implemented for positioning while volume beamforming was performed in postprocessing at a rate of, typically, a few volumes per second; the reconstruction rate decreased with the imaging depth, the number of compounded emissions, and the reconstruction sampling rate. 3-D rendering was performed using Amira software (Visualization Sciences Group, Burlington, MA).

Image formation

A single framework consisting of virtual sources positioned behind the probe was used for compounding emissions (Fig. 1). More specifically, synthetic beamforming was performed using virtual sources forming a virtual array located behind the probe (Fig. 1A). For each source, a physical subaperture and a set of delays were computed (Fig. 1B). Emissions from individual sources were performed sequentially, and the radio-frequency data was recorded for each element of the entire physical probe. Volumes were beamformed using delay-and-sum algorithms for each virtual source and subsequently coherently compounded to form a final, high quality volume. Virtual arrays can be tailored to adjust resolution, contrast, signal-to-noise ratio, volume rate, and the field of view in a quasi-continuous fashion, therefore allowing for the selection of the optimal imaging sequence for a specific application (Lockwood et al., 1998; Montaldo et al., 2009; Nikolov, 2001; Nikolov et al., 2010; Clement Papadacci et al., 2014).

Indeed, a number of trade-offs between contrast, resolution, volume rate and field of view exist. For example, as the number of sources is increased, the contrast and resolution improve but the volume rate decreases, and as the distance of the virtual array decreases, the field of view increases but the contrast decreases. More specifically, positioning virtual sources onto the probe itself is equivalent to standard synthetic beamforming, with a high resolution and large field of view, but resulting in a poor volume rate and signal-to-noise ratio at larger depths. As the virtual array is moved behind the probe (Fig. 1C), additional physical elements can be recruited to contribute to one emission (i.e., the subaperture) and therefore increased energy is propagated into the tissue and larger SNRs are obtained (Lockwood et al., 1998). The volume rate can also be adjusted by either increasing the pitch or decreasing the aperture of the virtual array up to the extreme case of using a single source (Provost et al., 2011b), which is useful for applications requiring very high volume rates such as Ultrafast Doppler or Shear-Wave Imaging. Placing sources farther behind the probe leads to larger emission subapertures and a smaller field of view. Indeed, a virtual array at infinity (or very far, e.g., at 60 000 mm in this study) results in the emission of plane waves (Fig. 1D) with an imaging field of view corresponding to the 2-D aperture of the physical probe.

Blood flow and motion estimation were performed by generalizing standard methods reported in previous studies. Namely, the Kasai algorithm (Kasai et al., 1985) was used to estimate motion in phantoms and in tissues with a half-wavelength spatial sampling. Blood flow was estimated by first applying a high-pass filter to the baseband data and then, for each individual voxel, Power Doppler was obtained by integrating the power-spectral density, Pulsed Doppler was obtained by computing the short-time Fourier transform, and Color Doppler maps were obtained by estimating the first moment of the voxel-specific Pulsed-Doppler spectrogram.

Experimental Setup

Improvement in resolution was quantified as a function of the number of elements in the virtual array using a customized resolution phantom consisting of 1-mm metallic beads embedded in gelatin. This phantom contained a single layer containing 25 beads and was

imaged at 5 different depths to generate a synthetic resolution phantom. Resolution was quantified by measuring the width at −3dB of the main lobes for each bead. Contrast was quantified in a heart-mimicking phantom (067, CIRS, VA) by calculating the tissue-to-cavity ratio in a few voxels at a given depth as a function of the number of sources, as well as in the common carotid of a healthy volunteer near the bifurcation. Shear-Wave Imaging was performed using two probes: the 2-D matrix array, was used to track the propagation of the shear wave in a 1.92-kPa phantoms, whereas a standard 6-MHz, 1-D linear array (L10-2, Supersonic Imaging, Aix-en-Provence, France), located approximately 2 cm away from the 2-D array generated three 100-μs radiation force 'pushes' at approximately 2 cm away from the center of the 2-D matrix array. The three push focal zones generated a Mach cone and thus an approximately conical shear wave. Note that the system could be used with the matrix array as a single probe to generate radiation force and to perform ultrafast imaging, but the experiment was not conducted in this study in order to avoid potentially damaging our customized probe. 3-D Ultrafast Doppler Imaging was demonstrated by imaging the heart of a normal subject and the feasibility of simultaneous 3-D Ultrafast Doppler and 3-D Tissue Doppler was shown through the observation of the propagation of the pulse wave in the carotid artery undergoing pulsatile flow.

Results

Resolution and Contrast

Fig. 2A shows the resolution phantom imaged using 1 and 81 virtual sources, respectively. One can observe an improvement in lateral resolution as the number of sources increased. Interestingly, however, as 3-D focusing was performed at every voxel in receive, the resolution remained high, even when using a single emission.

In terms of contrast, however, the situation was different: Fig. 2B (supplementary video 1) shows the improvement in contrast between the cavity and the tissue in a heart-mimicking phantom for varying depths as the number of coherently-compounded sources increased. The virtual array used had a pitch of 0.53 mm and a subaperture of 16×16 physical elements. Sources were added from the center as shown in figure 3. We can observe, as was the case in 2D (Clement Papadacci et al., 2014), a rapid increase in contrast with the number of sources. Indeed, the first 10-dB increase in contrast could be obtained using 5 sources instead of one. To obtain a 20-dB increase, 9 sources had to be added, for a total of 16. A plateau was reached near the 30-dB mark, when 36 or more sources were used.

Similar results were obtained in vivo. Fig. 2C shows the contrast improvement associated with the use of multiple virtual sources in the carotid of a normal subject in vivo. The 9×9 virtual array used was positioned at infinity behind the probe to generate plane waves angulated from −8 to 8 degrees. A similar behavior was observed: a rapid increase in contrast occurred for the first few sources added before reaching a plateau. Notably, the plateau obtained corresponded to a smaller increase in contrast when compared against the phantom experiment of Fig. 3A and occurred at approximately 16 sources. This was, however, expected, as the motion of the tissue and blood, along with the hand motion of the sonographer, reduced the contrast enhancing properties of coherent compounding, especially

when using a large virtual array requiring long acquisition times (8.4 ms for 81 sources with a 4-cm depth, i.e., 118 volumes/s).

3-D Shear-Wave Imaging

3-D Shear-Wave Imaging was performed using one virtual source located 2 cm behind the probe and a subaperture corresponding to the entire physical aperture at a rate of 3000 volumes/s. Fig. 3 (supplementary video 2) shows the propagation of the shear wave over a 3-cm distance from three different angles, i.e., from an approximately isometric view (Fig. 3A), from the top (Fig. 3B), and from the side (Fig. 3C). Its velocity was found to be approximately 0.8 m/s, in accordance with the stiffness of the phantom used (Young's Modulus equal to 1.92 kPa).

3-D Ultrafast Doppler Imaging

Blood flow estimation was performed in the apical view of the heart of a healthy volunteer at 2325 volumes/s and using a one-source acquisition. A single ultrafast acquisition allowed the computation, in post-processing, of Color Doppler for each voxel of the volume. Color Doppler maps in which the Power Doppler data was used as a mask to perform the automatic 3-D segmentation of the ventricles are shown in Fig. 4 (supplementary video 3). The Color Doppler ciné-loops in multiple complementary views and describing the different phases of the cardiac cycle in the left ventricle are shown: pre-ejection, ejection, rapid filling, diastasis, and atrial systole.

Finally, Fig. 5 (supplementary video 4) demonstrates how the high-quality acquisition using 81 sources can be used to to display 1) the anatomy using a compounded B-mode, and combined to a one-source acquisition to quantify 2) Blood flow using Ultrafast Doppler Imaging and 3) motion of the carotid walls using Tissue Doppler. The Color Doppler maps were segmented using the Power Doppler data and overlaid onto the high-quality B-mode shown in Fig. 1C and acquired immediately after the 1-s one-source acquisition sequence at 3000 volumes/s. The Tissue Doppler was overlaid onto the B-mode images and segmented by applying a dilation operation onto the Power Doppler mask. The bifurcation of the carotid could be identified and fully characterized as it was visible both in the high-quality B-mode and in the Doppler ciné-loop. For instance, one can observe the Power Doppler Spectrum at any voxel, including at the entrance and exits of the bifurcation (Fig. 5). Fig. 5 also shows the propagation of the pulse wave in the carotid wall (Couade et al., 2010; Luo et al., 2012); which is a flow velocity, pressure, and diameter waves generated at the ejection phase of the left ventricle (Nichols et al., 2011).

Discussion

In this study, we have demonstrated the feasibility of 3-D Ultrafast Ultrasound Imaging in humans in vivo. More specifically, we have shown that by using a virtual array located behind the probe, it is possible to achieve high contrast and good resolution with a small number of coherently compounded emissions, hence allowing for the imaging of thousands of volumes per second. Such high volume rates allow, in turn, for the accurate mapping in entire 3D volumes of Color Doppler, Power Doppler, Pulsed Doppler, and Tissue Doppler of

each individual voxel. By implementing each algorithm on GPUs, it was shown possible to obtain these quantities in real-time or quasi-real-time depending on the required imaging depth and spatial sampling.

Fig. 2 (supplementary video 1) demonstrated that coherent compounding can be used to achieve an optimal, application-dependent trade-off between contrast, resolution, and volume rate. Fig. 3 (supplementary video 2) demonstrated the feasibility of both 3-D Tissue Doppler and Shear-Wave Imaging for the mechanical characterization of tissues in 3 dimensions. Fig. 4 (supplementary video 3) demonstrated the feasibility of Ultrafast Doppler Imaging can be performed in the challenging clinical setting of cardiac imaging in which we were able to fully characterize all the phases of the cardiac cycle. Finally, Fig. 5 (supplementary video 4) shows that 3-D Ultrafast Doppler Imaging, 3-D Tissue Doppler can be performed in the carotid in a single acquisition and overlaid onto a high-quality B-mode obtained at approximately 100 volumes/s, which is more than sufficient for anatomical imaging.

3-D Ultrafast Ultrasound Imaging could potentially revolutionize current clinical practices. Indeed, we have shown that by using 3-D Ultrafast Ultrasound Imaging, blood flow can be visualized and quantified, e.g., in the totality of the carotid bifurcation, in order to identify the presence of abnormalities. Perhaps more importantly, the techniques detailed herein can be applied, theoretically, to any other organ. For example, in the heart, it paves the way to the complete, quantitative, 3-D mapping of the blood flow in all 4 cavities simultaneously for the identification of abnormal patterns, which is the subject of on-going studies in our group.

Limitations to the technique include the reduced energy transmitted to the tissues, especially when a large field of view is needed, as it requires the use of spherical waves emerging from virtual sources located close to the probe. Indeed, the ultrasound pulse energy decreases as the cube of the depth, without taking into account attenuation. This limitation can, however, be overcome by using the coherent compounding of multiple emissions, coded excitations, pre-amplified probes, or the development of higher-powered pulsers. Indeed, using compounded diverging waves allows for the safe propagation of large cumulative energy while insuring limited tissue heating and small instantaneous local pressure, both of which are at the source of known potential adverse bioeffects. Moreover, the results of the resolution experiment of Fig. 2A are to be considered qualitatively only, as the metallic beads used were not sufficiently small against the focal zone size to provide quantitative resolution results; a complete quantitative characterization resolution study is the object of on-going work.

One other important feature of 3D ultrafast imaging is the simultaneous acquisition of all RF data within the observation volume. Such simultaneous and large field of view acquisition will permit to improve the acquired cineloops in postprocessing. For example, aberration corrections techniques, known to be of limited interest in 2D as they do not account for out-of-plane aberrations will be applied in a much better way to improve the quality of post-processed cineloops. Moreover, motion compensation algorithms, for example in cardiac

Europe PMC Funders Author Manuscripts

applications, already demonstrated recently in 2D (Denarie et al 2013) could be straigthforwardly extended to 3D ultrafast acquisitions.

In conclusion, we have demonstrated the feasibility of 3-D Ultrasound Ultrafast Imaging in humans in vivo, which is a novel approach for the simultaneous quantitative, functional, and anatomical imaging of tissues in 3 dimensions at very high volume rates. Such a technology allows for the mapping of blood flow and tissue motion in entire 3-D fields of view and promises to enhance the current limitations of 2-D echography in terms of inter- and intra-observer variability and to generate a host of novel 3-D applications ranging from brain activation mapping and cardiac electrophysiology to ultrasound-based angiography and 3-D shear-wave imaging of tumors.

Supplementary Material

Refer to Web version on PubMed Central for supplementary material.

Acknowledgements

This work was supported by the European Research Council under the European Union's Seventh Framework Programme (FP/2007-2013) / ERC Grant Agreement n°311025 and by LABEX WIFI (Laboratory of Excellence ANR-10-LABX-24) within the French Program "Investments for the Future" under reference ANR-10-IDEX-0001-02 PSL. J.P. is funded by a Marie Curie International Incoming Fellowship.

References

Bercoff J, Tanter M, Fink M. Supersonic shear imaging: a new technique for soft tissue elasticity mapping. IEEE Trans. Ultrason. Ferroelectr. Freq. Control. 2004; 51:396–409. doi:10.1109/TUFFC.2004.1295425. [PubMed: 15139541]

Couade M, Pernot M, Prada C, Messas E, Emmerich J, Bruneval P, Criton A, Fink M, Tanter M. Quantitative Assessment of Arterial Wall Biomechanical Properties Using Shear Wave Imaging. Ultrasound Med. Biol. 2010; 36:1662–1676. doi:10.1016/j.ultrasmedbio.2010.07.004. [PubMed: 20800942]

Couade, M.; Pernot, M.; Tanter, M.; Messas, E.; Bel, A.; Ba, M.; Hagege, A-A.; Fink, M. Ultrafast imaging of the heart using circular wave synthetic imaging with phased arrays. Ultrasonics Symposium (IUS), 2009 IEEE International; Presented at the Ultrasonics Symposium (IUS), 2009 IEEE International; 2009; p. 515-518.doi:10.1109/ULTSYM.2009.5441640

Demené C, Pernot M, Biran V, Alison M, Fink M, Baud O, Tanter M. Ultrafast Doppler reveals the mapping of cerebral vascular resistivity in neonates. J. Cereb. Blood Flow Metab. 2014 doi:10.1038/jcbfm.2014.49.

Denarie B, Bjastad T, Torp H. Multi-line transmission in 3-D with reduced crosstalk artifacts: a proof of concept study. IEEE Trans. Ultrason. Ferroelectr. Freq. Control. 2013; 60:1708–1718. doi:10.1109/TUFFC.2013.2752. [PubMed: 25004541]

Dort, S.; Muth, S.; Swillens, A.; Segers, P.; Cloutier, G.; Garcia, D. Vector flow mapping using plane wave ultrasound imaging. Ultrasonics Symposium (IUS), 2012 IEEE International; Presented at the Ultrasonics Symposium (IUS), 2012 IEEE International; 2012; p. 330-333.doi:10.1109/ULTSYM.2012.0081

Ekroll IK, Swillens A, Segers P, Dahl T, Torp H, Lovstakken L. Simultaneous quantification of flow and tissue velocities based on multi-angle plane wave imaging. IEEE Trans. Ultrason. Ferroelectr. Freq. Control. 2013; 60:727–738. doi:10.1109/TUFFC.2013.2621. [PubMed: 23549533]

Fink M, Tanter M. Multiwave imaging and super resolution. Phys. Today. 2010; 63:28–33. doi:10.1063/1.3326986.

Fujikura K, Luo J, Gamarnik V, Pernot M, Fukumoto R, Tilson MD, Konofagou EE. A Novel Noninvasive Technique for Pulse-Wave Imaging and Characterization of Clinically-Significant Vascular Mechanical Properties In Vivo. Ultrason. Imaging. 2007; 29:137–154. doi: 10.1177/016173460702900301. [PubMed: 18092671]

Hazard CR, Lockwood GR. Theoretical assessment of a synthetic aperture beamformer for real-time 3-D imaging. IEEE Trans. Ultrason. Ferroelectr. Freq. Control. 1999; 46:972–980. doi: 10.1109/58.775664. [PubMed: 18238502]

Honjo Y, Hasegawa H, Kanai H. Two-Dimensional Tracking of Heart Wall for Detailed Analysis of Heart Function at High Temporal and Spatial Resolutions. Jpn. J. Appl. Phys. 2010; 49

Kasai C, Namekawa K, Koyano A, Omoto R. Real-Time Two-Dimensional Blood Flow Imaging Using an Autocorrelation Technique. IEEE Trans. Sonics Ultrason. 1985; 32:458–464. doi:10.1109/T-SU.1985.31615.

Konofagou E, Lee W-N, Luo J, Provost J, Vappou J. Physiologic Cardiovascular Strain and Intrinsic Wave Imaging. Annu. Rev. Biomed. Eng. 2011; 13:477–505. doi:10.1146/annurev-bioeng-071910-124721. [PubMed: 21756144]

Lee W-N, Pernot M, Couade M, Messas E, Bruneval P, Bel A, Hagege AA, Fink M, Tanter M. Mapping Myocardial Fiber Orientation Using Echocardiography-Based Shear Wave Imaging. Med. Imaging IEEE Trans. On. 2012; 31:554–562. doi:10.1109/TMI.2011.2172690.

Lockwood GR, Talman JR, Brunke SS. Real-time 3-D ultrasound imaging using sparse synthetic aperture beamforming. IEEE Trans. Ultrason. Ferroelectr. Freq. Control. 1998; 45:980–988. doi: 10.1109/58.710573. [PubMed: 18244252]

Luo J, Li RX, Konofagou EE. Pulse wave imaging of the human carotid artery: an in vivo feasibility study. IEEE Trans. Ultrason. Ferroelectr. Freq. Control. 2012; 59:174–181. doi:10.1109/TUFFC.2012.2170. [PubMed: 22293749]

Mace E, Montaldo G, Cohen I, Baulac M, Fink M, Tanter M. Functional ultrasound imaging of the brain. Nat Meth. 2011; 8:662–664. doi:10.1038/nmeth.1641.

Macé E, Montaldo G, Cohen I, Baulac M, Fink M, Tanter M. Functional ultrasound imaging of the brain. Nat. Methods. 2011; 8:662–664. doi:10.1038/nmeth.1641. [PubMed: 21725300]

Montaldo G, Tanter M, Bercoff J, Benech N, Fink M. Coherent plane-wave compounding for very high frame rate ultrasonography and transient elastography. IEEE Trans. Ultrason. Ferroelectr. Freq. Control. 2009; 56:489–506. doi:10.1109/TUFFC.2009.1067. [PubMed: 19411209]

Nichols, W.; O'Rourke, M.; Vlachopoulos, C. McDonald's Blood Flow in Arteries, Sixth Edition: Theoretical, Experimental and Clinical Principles. 6 edition. CRC Press; London: 2011.

Nikolov, SI. Synthetic aperture tissue and flow ultrasound imaging. Orsted-DTU, Technical University of Denmark; Lyngby, Denmark: 2001.

Nikolov, SI.; Kortbek, J.; Jensen, JA. Practical applications of synthetic aperture imaging. 2010 IEEE Ultrasonics Symposium (IUS); Presented at the 2010 IEEE Ultrasonics Symposium (IUS); 2010; p. 350-358.doi:10.1109/ULTSYM.2010.5935627

Osmanski BF, Martin C, Montaldo G, Lanièce P, Pain F, Tanter M, Gurden H. Functional ultrasound imaging reveals different odor-evoked patterns of vascular activity in the main olfactory bulb and the anterior piriform cortex. NeuroImage. 2014; 95:176–184. doi:10.1016/j.neuroimage.2014.03.054. [PubMed: 24675645]

Papadacci C, Pernot M, Couade M, Fink M, Tanter M. High-contrast ultrafast imaging of the heart. IEEE Trans. Ultrason. Ferroelectr. Freq. Control. 2014; 61:288–301. doi:10.1109/TUFFC.2014.6722614. [PubMed: 24474135]

Papadacci C, Pernot M, Couade M, Fink M, Tanter M. High Contrast Ultrafast Imaging of the Human Heart. IEEE Trans Ultrason Ferroelectr Freq Control. 2014; 61:288–301. [PubMed: 24474135]

Papadacci C, Tanter M, Pernot M, Fink M. Ultrasound backscatter tensor imaging (BTI): analysis of the spatial coherence of ultrasonic speckle in anisotropic soft tissues. IEEE Trans. Ultrason. Ferroelectr. Freq. Control. 2014; 61:986–996. doi:10.1109/TUFFC.2014.2994. [PubMed: 24859662]

Pernot M, Fujikura K, Fung-Kee-Fung SD, Konofagou EE. ECG-gated, Mechanical and Electromechanical Wave Imaging of Cardiovascular Tissues In Vivo. Ultrasound Med. Biol. 2007a; 33:1075–1085. doi:10.1016/j.ultrasmedbio.2007.02.003. [PubMed: 17507146]

Pernot M, Fujikura K, Fung-Kee-Fung SD, Konofagou EE. ECG-gated, Mechanical and Electromechanical Wave Imaging of Cardiovascular Tissues In Vivo. Ultrasound Med. Biol. 2007b; 33:1075–1085. doi:10.1016/j.ultrasmedbio.2007.02.003. [PubMed: 17507146]

Perrin DP, Vasilyev NV, Marx GR, del Nido PJ. Temporal Enhancement of 3D Echocardiography by Frame Reordering. JACC Cardiovasc. Imaging. 2012; 5:300–304. doi:10.1016/j.jcmg.2011.10.006. [PubMed: 22421177]

Provost J, Gambhir A, Vest J, Garan H, Konofagou EE. A clinical feasibility study of atrial and ventricular electromechanical wave imaging. Heart Rhythm. 2013; 10:856–862. doi:10.1016/j.hrthm.2013.02.028. [PubMed: 23454060]

Provost J, Lee W-N, Fujikura K, Konofagou EE. Electromechanical Wave Imaging of Normal and Ischemic Hearts in Vivo. IEEE Trans. Med. Imaging. 2010; 29:625–635. doi:10.1109/TMI.2009.2030186. [PubMed: 19709966]

Provost J, Lee W-N, Fujikura K, Konofagou EE. Imaging the electromechanical activity of the heart in vivo. Proc. Natl. Acad. Sci. USA. 2011a; 108:8565–8570. doi:10.1073/pnas.1011688108. [PubMed: 21571641]

Provost J, Nguyen VT-H, Legrand D, Okrasinski S, Costet A, Gambhir A, Garan H, Konofagou EE. Electromechanical wave imaging for arrhythmias. Phys. Med. Biol. 2011b; 56:L1–L11. doi:10.1088/0031-9155/56/22/F01. [PubMed: 22024555]

Provost J, Thiébaut S, Luo J, Konofagou EE. Single-Heartbeat Electromechanical Wave Imaging with Optimal Strain Estimation Using Temporally-Unequispaced Acquisition Sequences. Phys. Med. Biol. 2012; 57:1095–1112. [PubMed: 22297208]

Sandrin L, Catheline S, Tanter M, Hennequin X, Fink M. Time-resolved pulsed elastography with ultrafast ultrasonic imaging. Ultrason. Imaging. 1999; 21:259–272. [PubMed: 10801211]

Sandrin L, Fourquet B, Hasquenoph J-M, Yon S, Fournier C, Mal F, Christidis C, Ziol M, Poulet B, Kazemi F, Beaugrand M, Palau R. Transient elastography: a new noninvasive method for assessment of hepatic fibrosis. Ultrasound Med. Biol. 2003; 29:1705–1713. doi:10.1016/j.ultrasmedbio.2003.07.001. [PubMed: 14698338]

Skaug TR, Amundsen BH, Hergum T, Urheim S, Torp H, Haugen BO. Quantification of aortic regurgitation using high-pulse repetition frequency three-dimensional colour Doppler. Eur. Heart J. Cardiovasc. Imaging. 2014; 15:615–622. doi:10.1093/ehjci/jet255. [PubMed: 24344195]

Tanter M, Bercoff J, Athanasiou A, Deffieux T, Gennisson J-L, Montaldo G, Muller M, Tardivon A, Fink M. Quantitative Assessment of Breast Lesion Viscoelasticity: Initial Clinical Results Using Supersonic Shear Imaging. Ultrasound Med. Biol. 2008; 34:1373–1386. doi:10.1016/j.ultrasmedbio.2008.02.002. [PubMed: 18395961]

Tanter M, Bercoff J, Sandrin L, Fink M. Ultrafast compound imaging for 2-D motion vector estimation: application to transient elastography. IEEE Trans. Ultrason. Ferroelectr. Freq. Control. 2002; 49:1363–1374. doi:10.1109/TUFFC.2002.1041078. [PubMed: 12403138]

Tanter M, Fink M. Ultrafast imaging in biomedical ultrasound. IEEE Trans. Ultrason. Ferroelectr. Freq. Control. 2014; 61:102–119. doi:10.1109/TUFFC.2014.6689779. [PubMed: 24402899]

Udesen J, Gran F, Hansen KL, Jensen JA, Thomsen C, Nielsen MB. High frame-rate blood vector velocity imaging using plane waves: Simulations and preliminary experiments. IEEE Trans. Ultrason. Ferroelectr. Freq. Control. 2008; 55:1729–1743. doi:10.1109/TUFFC.2008.858. [PubMed: 18986917]

Vappou J, Luo J, Konofagou EE. Pulse Wave Imaging for Noninvasive and Quantitative Measurement of Arterial Stiffness In Vivo. Am. J. Hypertens. 2010; 23:393–398. doi:10.1038/ajh.2009.272. [PubMed: 20094036]

Wang S, Lee W-N, Provost J, Luo J, Konofagou EE. A composite high-frame-rate system for clinical cardiovascular imaging. Ultrason. Ferroelectr. Freq. Control IEEE Trans. On. 2008; 55:2221–2233.

Yiu B, Lai S, Yu A. Vector projectile imaging: time-resolved dynamic visualization of complex flow patterns. Ultrasound Med. Biol. 2014; 40:2295–2309. [PubMed: 24972498]

Europe PMC Funders Author Manuscripts

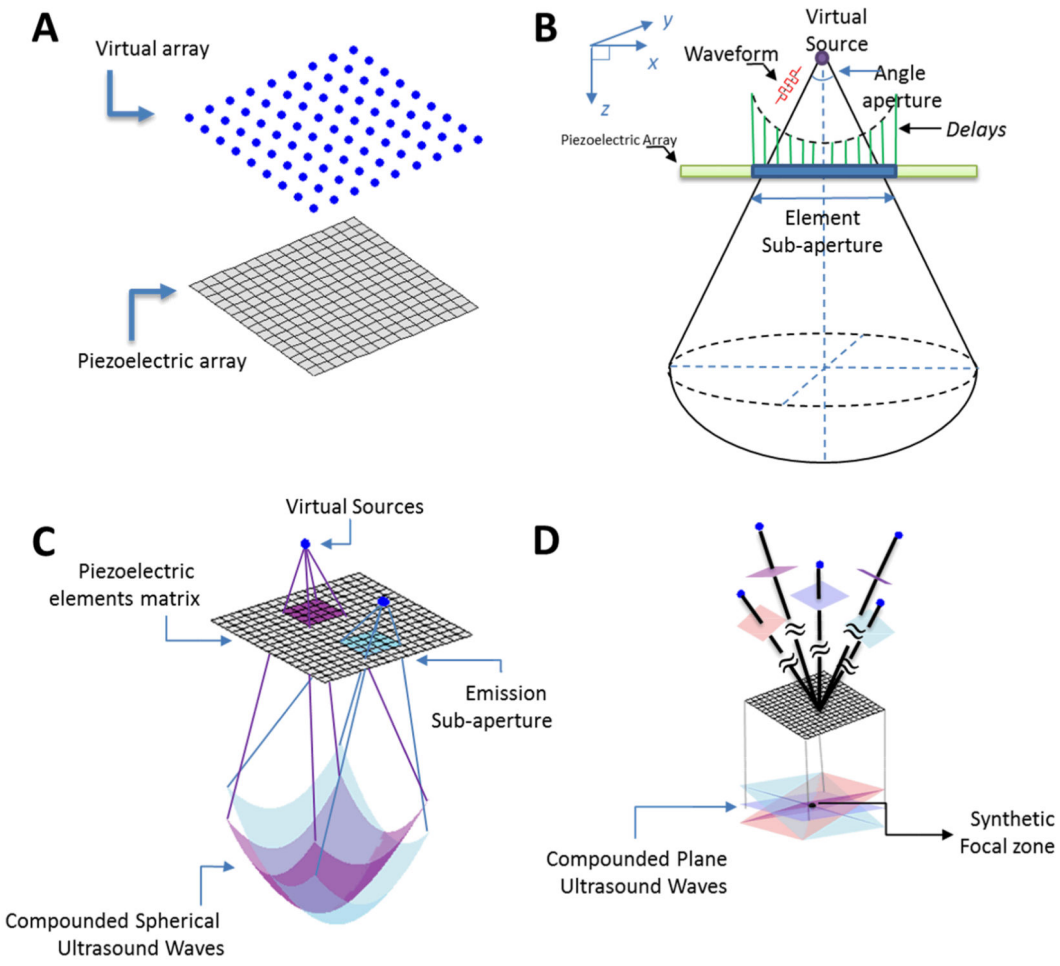

Figure 1. 3-D Ultrafast Ultrasound Imaging Framework

A Acquisitions are defined by a virtual array located behind the probe, which is then used to synthetically form an entire volume. **B** For each individual source, delays are computed and a sub-aperture is defined. **C** When virtual sources are located near the physical probe, the sub-aperture used is smaller and the curvature of the emitted waveform is increased, which results into the insonification of a large field-of-view at the cost of a lower propagated energy. **D** When sources are located far behind the probe, larger sub-apertures, and thus, emitted energy, at the cost of a smaller field of view. In the extreme case of sources located at infinity behind the probe, tilted plane waves are obtained.

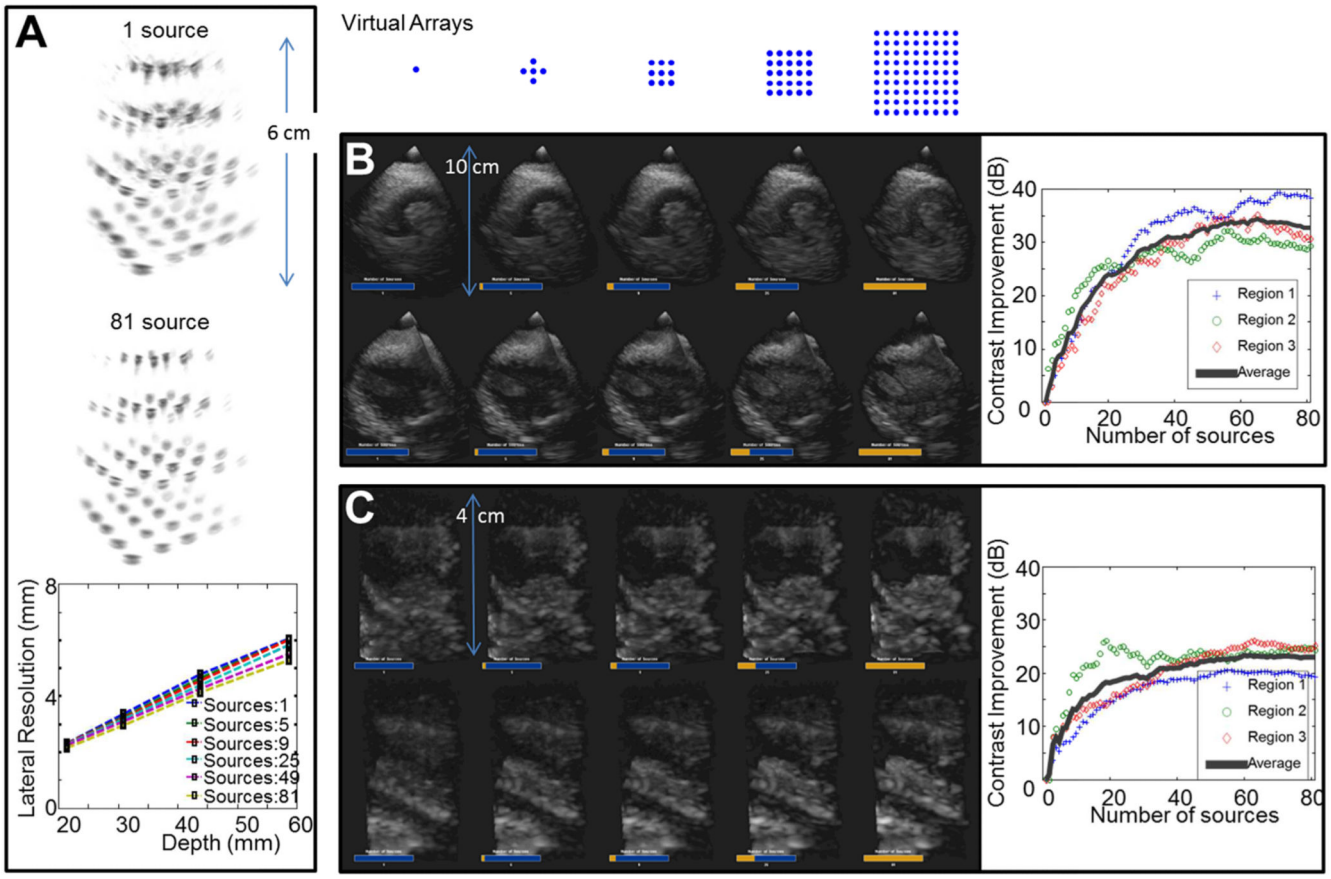

Figure 2. Resolution and Contrast

A An improvement in resolution is obtained when a larger virtual array is used. Indeed, as the number of virtual sources increases, the focal spot narrows and converges toward the optimal case of a focused emission in transmit and receive. Note that transmit-receive dynamic focusing does not lead to a spectacular improvement of the resolution compared to receive only focusing. The improvement in terms of contrast is more important; even a small number of emissions can significantly increase the contrast both in phantoms (**B**) and in the carotid of a human subject in vivo (**C**).

Europe PMC Funders Author Manuscripts

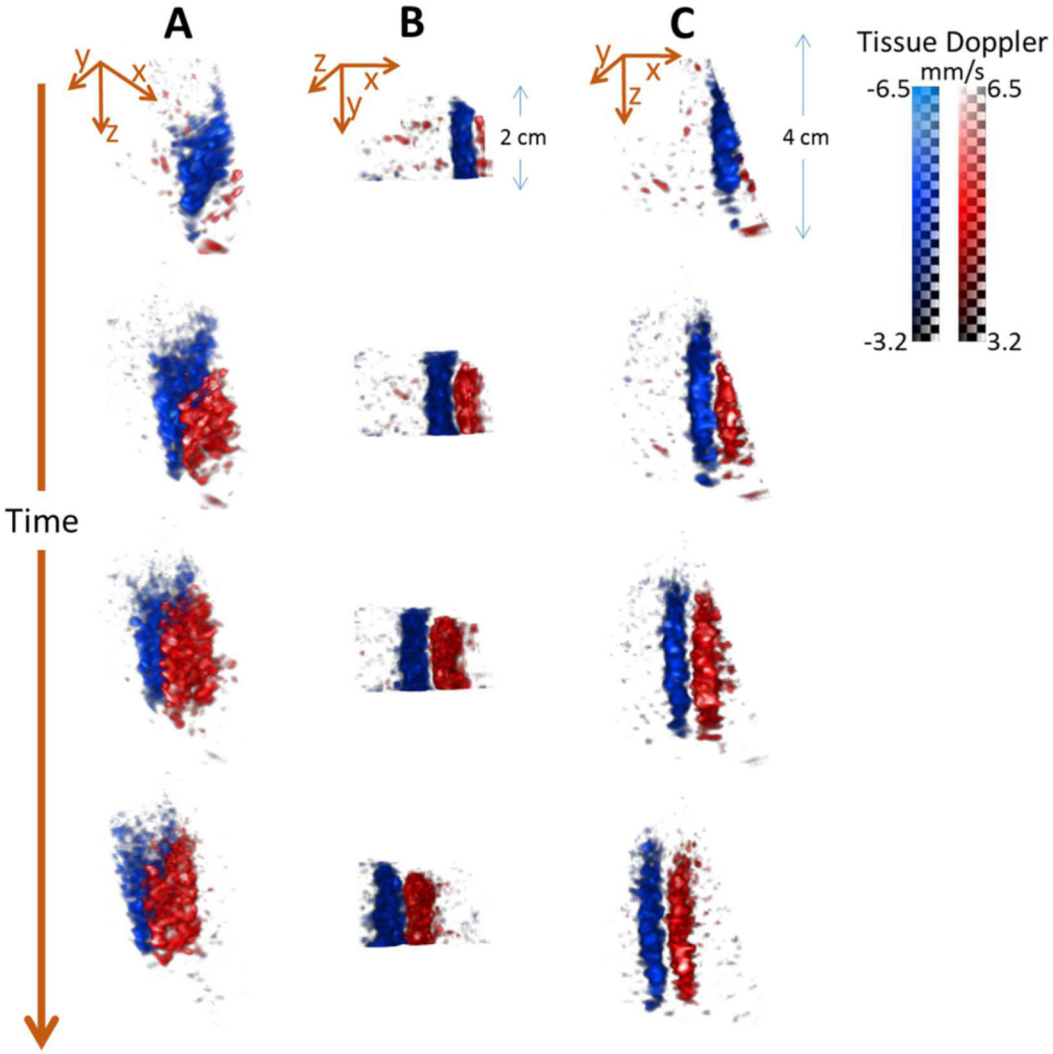

Figure 3. Motion estimation for 3-D Shear-Wave Imaging

Propagation of a shear-wave generated using radiation force from an **A** approximately isometric view, from **B** a top view and **C** a side view. The velocity of the wave was found to be approximately 0.8 m/s and corresponds to the stiffness of the phantom used (1.92 kPa).

Europe PMC Funders Author Manuscripts

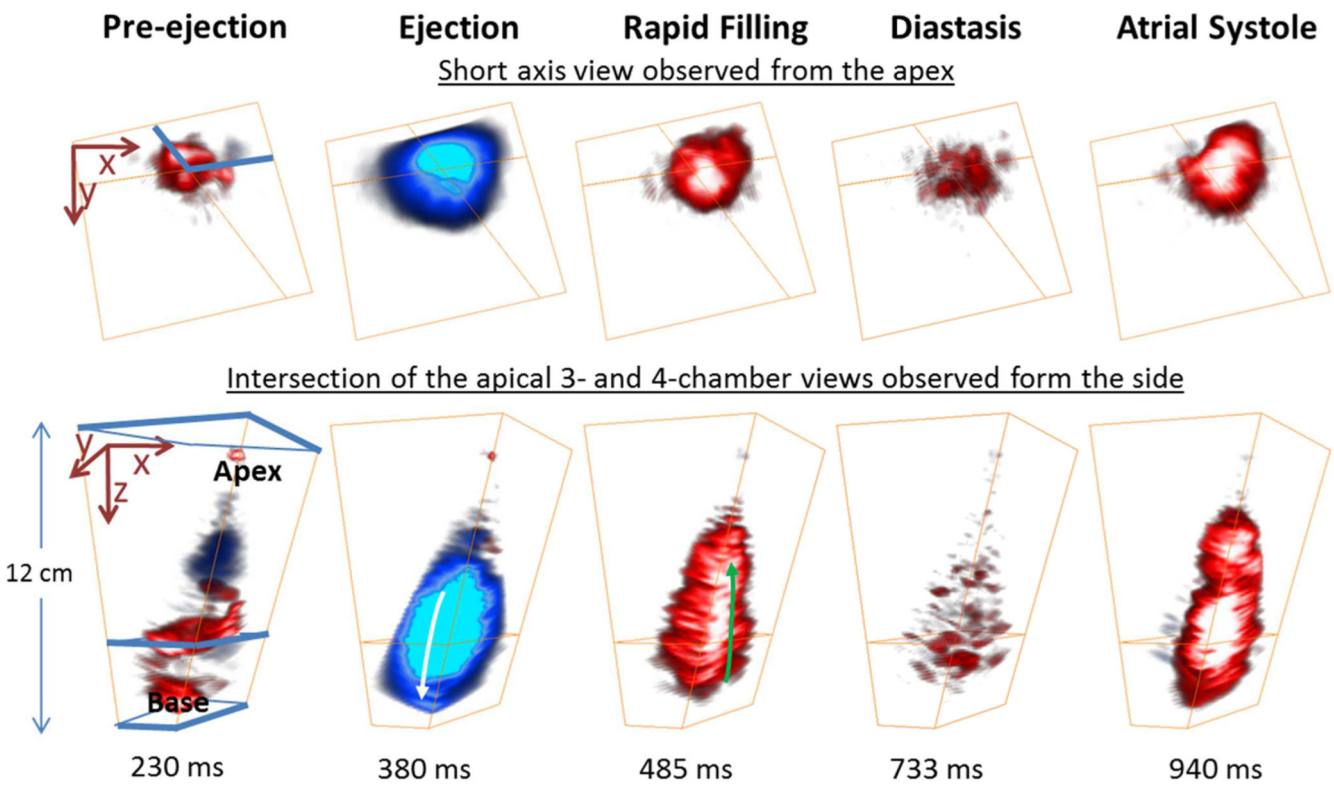

Figure 4. 3-D Ultrafast Doppler Imaging in the Heart

Blood flow in the left ventricle of a healthy volunteer during an entire cardiac cycle. After segmentation using the Power Doppler date, different well-known phases can be identified in the Color Flow Doppler ciné-loops such as ejection and rapid filling.

Europe PMC Funders Author Manuscripts

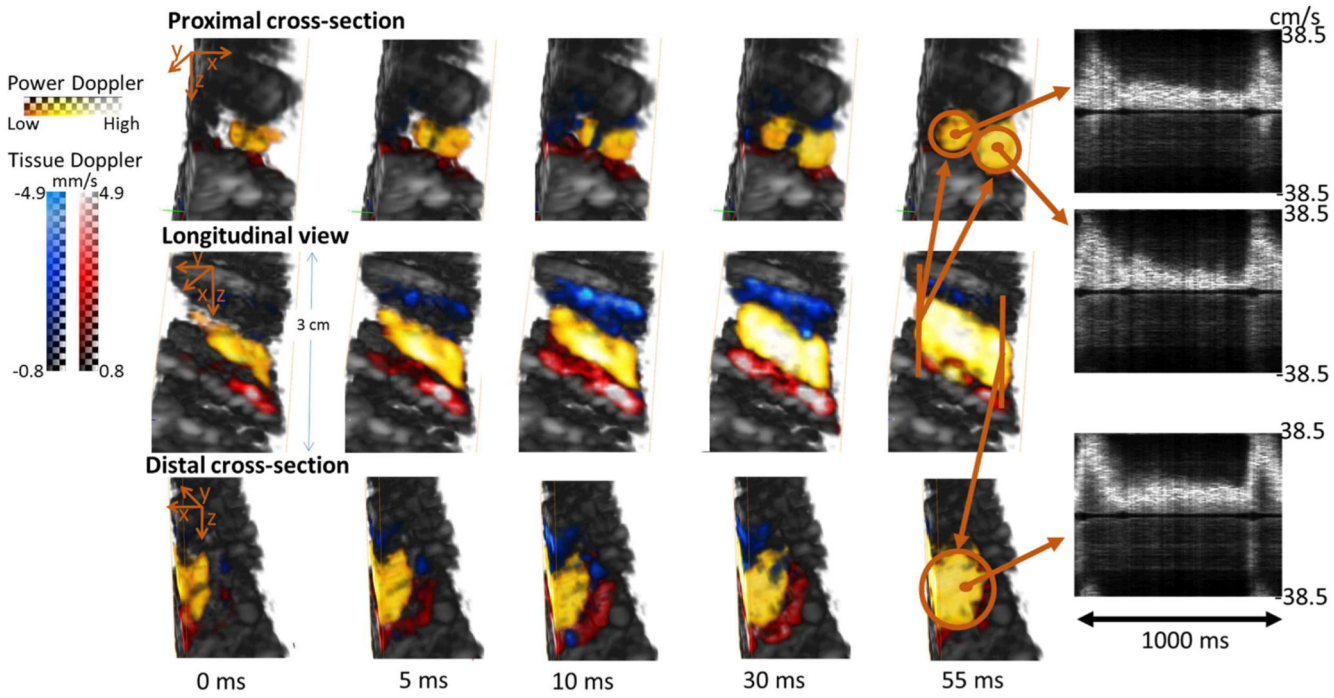

Figure 5. 3-D Ultrafast Doppler of the Carotid Bifurcation

Blood flow and tissue motion in the bifurcation of the carotid of a healthy volunteer overlaid onto a high quality B-mode volume during an entire cardiac cycle, along with quantitative blood flow shown for three regions at the entrance and exit of the bifurcation.

Europe PMC Funders Author Manuscripts